Composite Structures 132 (2015) 20–34

Contents lists available at ScienceDirect

Composite Structures

journal homepage: www.elsevier.com/locate/compstruct

Influence of arching action on shear behaviour of laterally restrained concrete slabs reinforced with GFRP bars

Y. Zheng *, C.H. Li, J.B. Yang, C. Sun

Department of Civil Engineering, Dongguan University of Technology, Dongguan, China

ARTICLE INFO

Article history:
Available online 16 May 2015

Keywords:
Arching action
GFRP
Concrete slab
Shear strength

ABSTRACT

This paper reveals the influence of arching action on the shear behaviour of glass fibre reinforced polymer (GFRP) reinforced laterally restrained concrete slabs in bridge decks. A total of seventeen full-size one-way concrete slabs were constructed and tested in this study. Those restrained test slabs represents typical full-scale dimensions of a real bridge deck slab 400 mm wide by 2400 mm long and 200 mm deep. The test variables were lateral restraint stiffness, reinforcement configuration and concrete strength. The behaviour of test slabs was discussed and the influence of those structural parameters on the amount of arching action was evaluated by comparing the results of different specimens. The test results showed that increasing the arching effect resulted in shear failure mode and larger shear strength. The experimental shear strengths of the restrained test slabs were compared with some theoretical predictions in the literatures. The results indicated that those theoretical methods yielded high conservative predictions. A theoretical model that takes into account the effect of arching action in the shear-strength prediction was proposed by the writers. This method provided accurate and slightly conservative predictions.

1. Introduction

It has been evident that corrosion of steel reinforcement constitutes one of major problems that shorten the service lifetime of concrete bridge decks [1,2]. One solution to this corrosion problem is the use of alternative materials to steel reinforcement that do not corrode, such as fibre reinforced polymer (FRP). Since glass fibre reinforced polymer (GFRP) is more economical than other available FRP (CFRP and AFRP), it is more attractive for infrastructure application and has been used as reinforcement in concrete bridge deck slabs for more than twenty years [3].

Currently, it is well established that the concrete bridge deck slabs can fail in shear, including punching shear failure and one-way shear failure, due to the in-plane restraints and the concentrated or distributed loads of large magnitude [4,5]. In addition, it has been recognised that an internal arching effect is induced as the slab deflects due to the horizontal restraints provided by the slab panel boundary conditions such as supporting beams, diaphragms and surrounding slabs [5]. This is known as arching action or compressive membrane action. In previous research, it was shown that this arching phenomenon had a strong effect on failure mode and ultimate capacity of GFRP reinforced concrete bridge deck slabs [5,6]. However, the majority of research on the shear behaviour of FRP reinforced concrete members has been concentrated on the simply supported beams or slabs [7]. The effect of arching action as a result of in-plane restraint was not taken into consideration except in the specimens with small span-to-depth ratio ($\leqslant 2.5$) [8]. Interestingly, the tests by authors showed that the failure mechanism of GFRP reinforced concrete deck slabs with large span-to-depth ratio ($\geqslant 2.5$) could be shear failure due to the significant arching action [5,9]. Therefore, an investigation of the shear behaviour of laterally restrained concrete slabs reinforced with GFRP bars should be carried out by taking into account the effect of arching action.

The aim of this paper is to study the shear behaviour of in-plane restrained GFRP reinforced concrete slabs in bridge deck structures. As shown in Fig. 1, a one-way spanning concrete slab strip with lateral restraints typical of a bridge deck slab is conducted in this study. A series of experimental tests were carried out to investigate the influence from some structural variables on the behaviour of those slabs, which included the degree of external restraints, concrete strengths, reinforcement percentages and reinforcing materials. After comparing the results of different test specimens, the

* Corresponding author at: Department of Civil Engineering, Dongguan University of Technology, Dongguan, Guangdong Province 523808, China. Tel.: +86 15899662977.

E-mail address: zhengy@dgut.edu.cn (Y. Zheng).

http://dx.doi.org/10.1016/j.compstruct.2015.05.028
0263-8223/

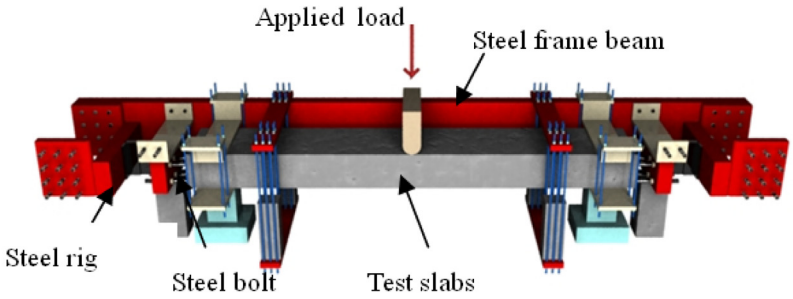

(a) Test slab and lateral restraint configuration

(b) A typical test specimen

Fig. 1. Test model.

influence of arching action on shear-strength and failure mode was discussed and presented. A understanding of the nature of shear behaviour of concrete deck slabs reinforced with GFRP bars can be extended. Subsequently, the shear-strengths from the test were compared to the theoretical predictions provided by some published shear-strength design methods and a model proposed by authors. It was shown that the theoretical method taking into consideration the effect of arching action proposed in this study gave reasonable agreement with the test results.

2. Background to shear behaviour of FRP reinforced concrete members

It is well known that the cracked reinforced concrete flexural member without shear reinforcement, such as concrete slabs, resists the applied shear stress by means of five structural mechanisms: (i) shear resistance of uncracked concrete; (ii) aggregate interlock; (iii) dowel action of the longitudinal reinforcement; (iv) residual tensile stress across the inclined crack; and (v) arching action [10]. As similar to the behaviour of steel reinforced concrete members, those five mechanisms are expected in FRP reinforced concrete members. Due to the relatively low modulus of elasticity of the FRP composite material, FRP reinforced concrete structures generally develop wider and deeper cracks compared to those reinforced with steel. Those cracks decrease the contribution to shear strength from the uncracked concrete due to the low depth of concrete in compression. The contribution of aggregate interlock and residual tensile stress can also be reduced by the large crack widths. Additionally, due to the relatively small transverse strength of FRP bars and relatively wider cracks, the contribution of dowel action may be negligible. Finally, the shear capacity of FRP reinforced concrete members is smaller than those reinforced with the same amount of steel bars. This is well reported by the findings from the experimental investigations [11]. In addition, the shear behaviour of FRP reinforced concrete slabs without shear reinforcement is potentially the dangerous case in shear prone applications due to the brittle nature of concrete and FRP reinforcing bars [10].

Since most research of the shear behaviour of FRP reinforced concrete members is carried out based on the simply supported

structures, the effect arching action was only taken into account in the shear-strength prediction model for the concrete members with a small shear span-to-depth ratio ($\leqslant 2.5$). The influence from the external restraints has not been considered in the existing theoretical prediction models. However, the test of GFRP reinforced concrete deck slabs by authors showed that the degree of in-plane restraint stiffness had a strong effect on failure mode and ultimate capacity [5]. Until now, few studies have investigated the influence of arching action set up as a result of restraints on the shear behaviour of GFRP reinforced concrete deck slabs. Therefore, this paper presents a comprehensive experimental an theoretical study of this arching effect on the shear behaviour of laterally restrained GFRP reinforced concrete slabs.

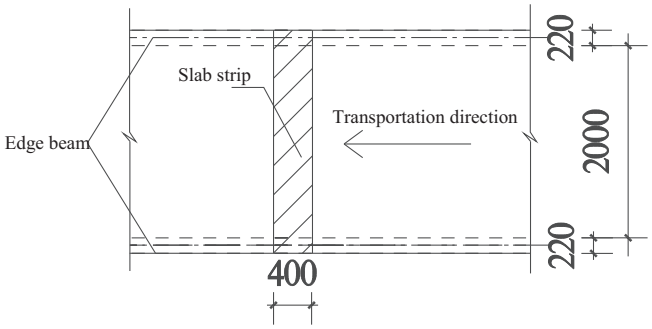

Fig. 2. One-way slab strip located in a global deck slab (unit: mm).

3. Experimental programme

3.1. Details of test slabs

The experimental test specimens were conducted to investigate the behaviour of one-way slabs representative of the typical sections of full scale bridge deck slabs, see Fig. 2. As illustrated in Fig. 3, the test slabs were 2400 mm long × 400 mm width × 200 mm deep. As shown in Table 1, the experimental programme is split into seven phases of testing. To achieve a noticeable increase in the arching capacity, the magnitude of lateral restraint stiffness were varied by three times (66 kN/mm, 190 kN/mm and 460 kN) as illustrated in Table 1 (Phases I to III). The values of the lateral restraint stiffness were adopted based on the previous test studies of bridge deck slabs [12] and laterally restrained concrete components [13]. Furthermore, three types of concrete strengths were used in each Phase of Phases I to III. In Phase IV, the horizontal restraint stiffness was removed to investigate the effect of the existence of horizontal restraints. In this experimental study, the influence of FRP reinforcement configuration, such as reinforcement percentage and position, were also investigated (see Phase V and VI). Finally, one slab reinforced with steel was fabricated and tested to study the effect of reinforcing material as shown in Table 1.

The test slabs were constructed by using normal-weight ready mixed concrete. The sand-coated glass FRP bars with 70% fibre content in a vinylester resin was used this test. Table 2 lists the material properties of the GFRP bars and steel bars used as longitudinal reinforcement. The test method for the GFRP bars was carried out according to the requirement of ACI 440-R06 [14] with the loading

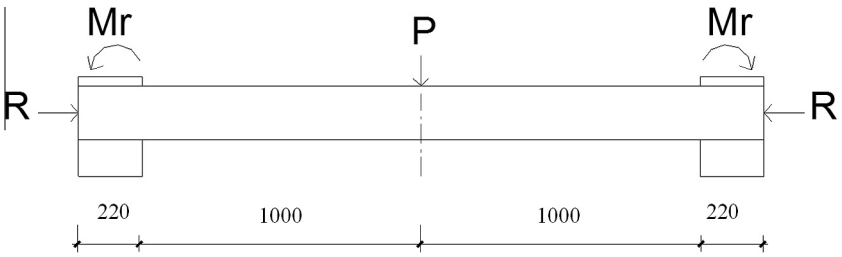

Fig. 3. Cross section of a test specimen (unit: mm).

Table 1
Experimental variables.

Phase	Model	Reinforcing material	f_{cu} *(N/mm^2)	ρ (%)	Reinforcement configuration	K_r (kN/mm)	Boundary condition	Failure load (kN)	Failure mode
I	SG1	GFRP	41	0.60	B/T 3φ12.70	460	FE + LR	187	SF
	SG2	GFRP	70	0.60	B/T 3φ12.70	460	FE + LR	199	SF
	SG3	GFRP	85	0.60	B/T 3φ12.70	460	FE + LR	205	SF
II	SG4	GFRP	41	0.60	B/T 3φ12.70	190	FE + LR	165	SF
	SG5	GFRP	62	0.60	B/T 3φ12.70	190	FE + LR	171	SF
	SG6	GFRP	84	0.60	B/T 3φ12.70	190	FE + LR	186	SF
III	SG7	GFRP	43	0.60	B/T 3φ12.70	66	FE + LR	155	SF
	SG8	GFRP	62	0.60	B/T 3φ12.70	66	FE + LR	162	SF
	SG9	GFRP	80	0.60	B/T 3φ12.70	66	FE + LR	176	SF
IV	SG10	GFRP	84	0.60	B/T 3φ12.70	0	FE	127	BF + RF
	SG11	GFRP	83	0.60	B/T 3φ12.70	0	SS	87	BF + RF
V	SG12	GFRP	85	0.60	B 3φ12.70	460	FE + LR	199	SF
	SG13	GFRP	88	1.00	C 3φ12.70	460	FE + LR	195	BF + SF
VI	SG14	GFRP	86	0.22	B/T 2φ9.53	460	FE + LR	195	SF
	SG15	GFRP	79	1.38	B 7φ12.70	460	FE + LR	210	SF
	SG16	GFRP	72	2.80	B 6φ19.05	460	FE + LR	215	SF
VII	SS1	Steel	80	0.60	B 4φ12.00	460	FE + LR	229	SF + YS

Boundary condition: FE = fixed end; LR = lateral restraint; SS = simply supported.
Reinforcement configuration: B = bottom; T = top; C = centre; N/A = no reinforcement.
Failure mode: SF = shear failure; BF = bending failure; RF = rupture failure; YS = yielding steel.

Table 2
Material properties of reinforcing bars.

Reinforcing material	Diameter (mm)	Yielding strength (N/mm^2)	Rupture strength (N/mm^2)	Elastic modulus (kN/mm^2)	Ultimate strain ($\mu\varepsilon$)
GFRP	9.53	–	760	40.8	18627
GFRP	12.7	–	690	40.8	16912
GFRP	19.05	–	620	40.8	15196
Steel	12	340	500	200	–

Fig. 4. Reinforcement layout in frame work before casting.

rate of 0.2 N/s. Fig. 4 shows a typical view of the reinforcement layout in the formwork. The reinforcement details of the test specimens and the reinforcement configurations are shown in Table 1. The clear cover of all the test slabs was 40 mm, except the test specimen coded as SG13.

3.2. Test apparatus and instrumentation

The effectiveness of in-plane thrust is dependent on the stiffness of restraints. A steel frame used in the previous test [6] provided the horizontal restraints and was analogous to end conditions of real slab system such as that of a bridge deck slab, as shown in Fig. 1. The lateral restraint stiffness is the combination of the axial stiffness of steel bolt and bending stiffness of steel rig as shown in Eq. (1).

$$\frac{1}{K_r} = \frac{1}{K_{\text{steel rig-bending stiffness}}} + \frac{1}{K_{\text{steel bolt-axial stiffness}}} \quad (1)$$

As illustrated in Fig. 3, a 430 × 25 mm line load was applied at the midspan for all the test slabs. The slabs were tested under three-point bending over a clear span of 2000 mm, giving a shear span-to-depth ratio of around 6. The strain gauges and displacement transducers were connected to a data acquisition system after the test specimens were positioned in the steel frame. The electrical resistant strain (ERS) gauges were embedded in reinforcing bars to assess the strain development in both the midspan and support locations (see Fig. 4). The vibrating wire strain gauges were located at the midspan, the one-fourth span and the support of sides of concrete slabs. As shown in Fig. 5, four linear variable-displacement

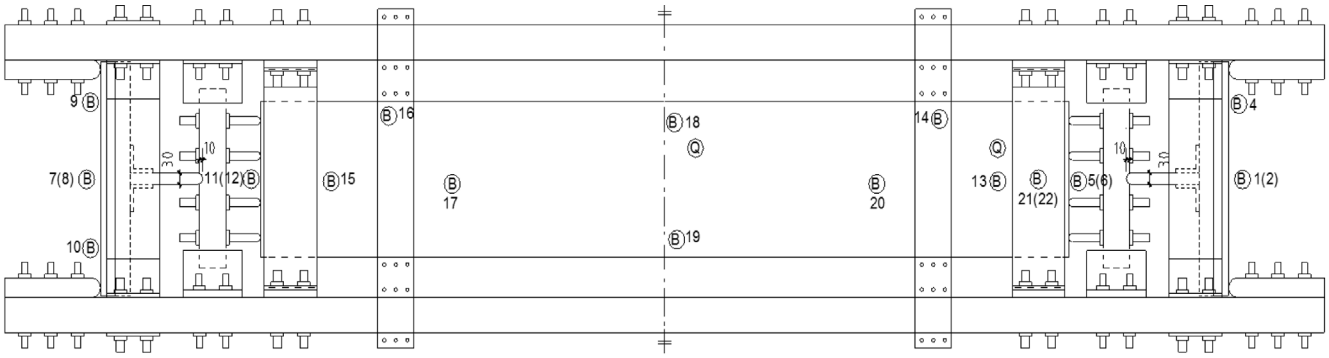

Ⓑ--Displacement transducer;

Ⓠ--Inclinometer

(a) Measurement position (to be continued)

(b) Details of dispacement transducers

Fig. 5. Measurement arrangement.

transducers (LVDT) were located at the midspan and one-fourth span of the concrete slabs to measure the vertical deflections of the test specimens. To study the arching effect, three displacement transducers were configured at the end of steel rigs to measure the horizontal displacements (see Fig. 5).

3.3. Test procedure

All the test slabs were accurately positioned in the restraining steel frame and attention was paid in positioning the slab relative to the loading frame to minimise the effect of eccentricity. In each

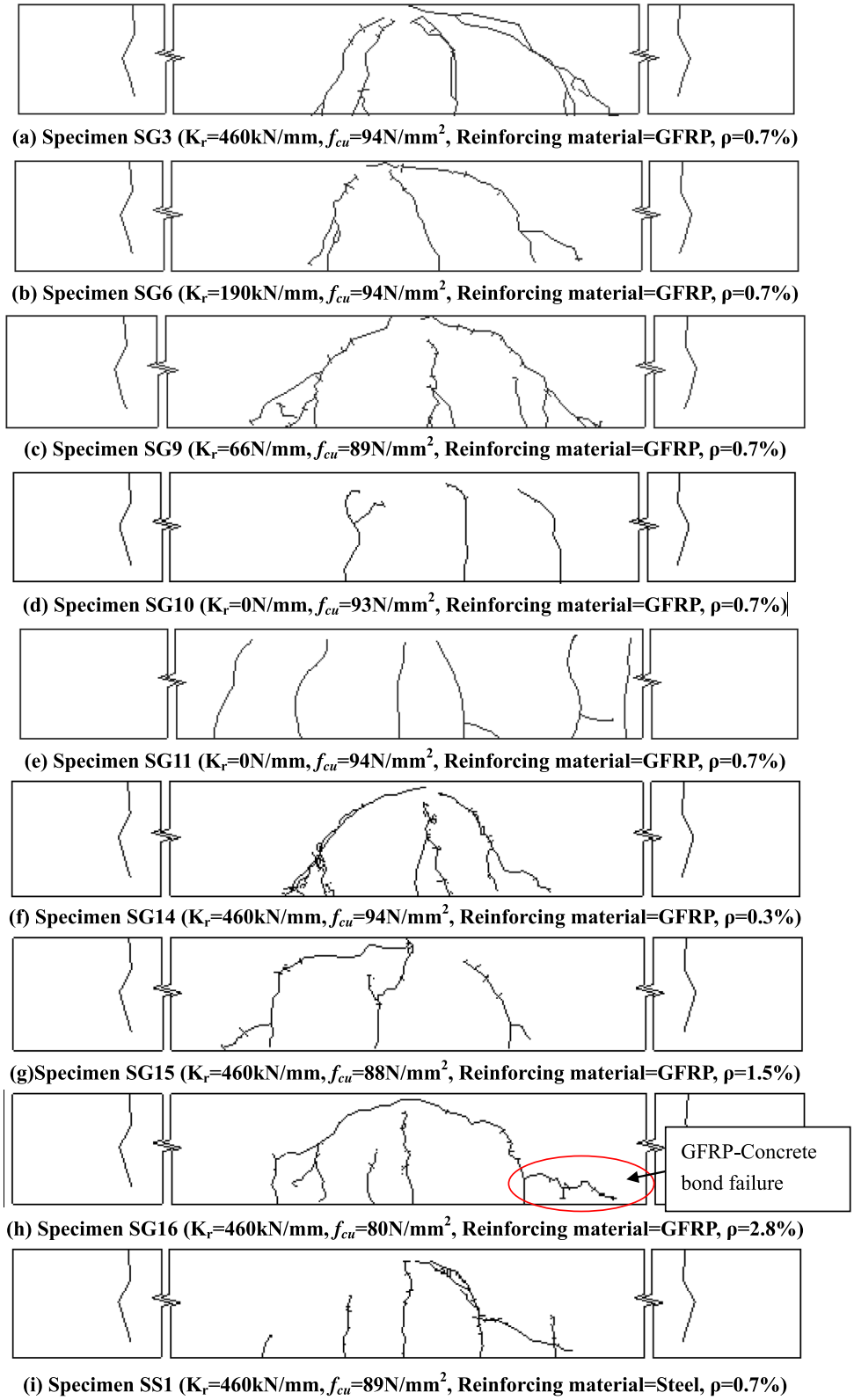

Fig. 6. Crack patterns of test slabs.

test specimen, two preliminary test loads were applied and the recovery was measured. Thereafter, the test slabs were loaded incrementally to failure. In the test process, deflections of the slabs, crack widths development, strains in GFRP bars and concrete slabs were measured for all the test specimens.

4. Experimental results

4.1. Crack patterns in the test slabs

Fig. 6 shows the propagation of crack patterns for the test slabs. It was illustrated that the few initial cracks were predominately vertical and perpendicular to the direction of the maximum stress induced by the bending moment and formed at an approximate service load of 50 kN. In the restrained test specimens, those flexural cracks did not penetrate into the compression zone. After the compressive zone depth of concrete slabs was reduced to 20–30 mm, those flexural cracks at the midspan did not propagate upwards the top surface. In addition, the initial cracks of the test slabs with lateral restraints remained narrow at this loading stage (around 60 kN). Furthermore, it was found that increasing the restraint stiffness resulted in smaller crack widths, which was similar to increasing the reinforcement percentage. Interestingly, the variation of reinforcing material could not influence the cracking pattern or cracking load significantly as shown in Fig. 6. Then, at higher loads, in the shear span, the cracks acquired some inclination towards the central zone, due to compressive stress in the shear span of the laterally restrained test specimens (see Fig. 6). Within the range of 50–60% of the ultimate load, the main diagonal crack formed, defining the direction of arching action (see Fig. 6). With the further loading, the GFRP-concrete bonding failure cracks were observed in the test slab (coded as SG16) with large reinforcement percentage (2.8%) (see Fig. 6h). After the loading level corresponding to around 80% of ultimate strengths, no more cracks appeared in all the test slabs.

The effect of boundary conditions on the failure mode is illustrated in Fig. 7. It was shown that the failure mode for restrained slabs was identified as diagonal shear-compression failure. In those slabs, diagonal cracks formed initially at the mid-depth of the slab in the direction of arching thrust propagating to the outside edge of loading beam and the inside edge of bearing plate at the support. With the development of this diagonal crack, the failure of those test slabs occurred with concrete crushing at the top surface. This type of shear-compression failure was typical for all the restrained concrete slabs, which had a large span-to-depth ratio (around 6), as shown in Table 1. Conversely, the vertical flexural cracks rather than the inclined shear cracks occurred in the slabs coded as SG11, which had no the external restraints, as shown in Fig. 7. Furthermore, it should be noted that increasing the lateral restraint stiffness or the reinforcement percentage both resulted in the significant shear behaviour in GFRP reinforced concrete slabs, see Figs. 6 and 7. Interestingly, no rupture of GFRP bars occurred in all the restrained concrete slabs even though the reinforcement percentage of those members were smaller than the balanced reinforcement percentage given by ACI 440-R06 [14] (around 1.25%). As it has been established that in-plane restrained slabs generally fail by concrete crushing due to the influence of arching action, replacing steel with FRP bars in restrained slabs does not require any additional provision as a concrete crushing failure mechanism occurs [6,15].

Fig. 8 compares the development of diagonal crack widths for the restrained slabs. It is of interest that the degree of lateral restraints and the FRP reinforcement percentage had a similar clear effect on controlling the diagonal crack width (see Fig. 8a and b). As shown in Fig. 8a, the crack widths were decreased about 58% when the lateral restraint stiffness were enhanced by three times at a loading level of 100 kN. At the same applied load, increasing the FRP reinforcement percentage from 0.22% to 2.8% resulted in decreasing the crack width by around 86% (see Fig. 8b). Conversely, the variation of concrete strengths could not affect the diagonal crack width significantly, see Fig. 8c.

4.2. Load vs. deflection response

Fig. 9 shows the midspan vertical defection versus the applied loads for the test slabs. It can be noted that all the slab specimens exhibited a nearly bilinear response up to failure. The first part up to the flexural cracking load (around 50–60 kN) was similar for all the test slabs representing the behaviour of the uncracked slab utilising the gross inertia of the concrete cross section, while the

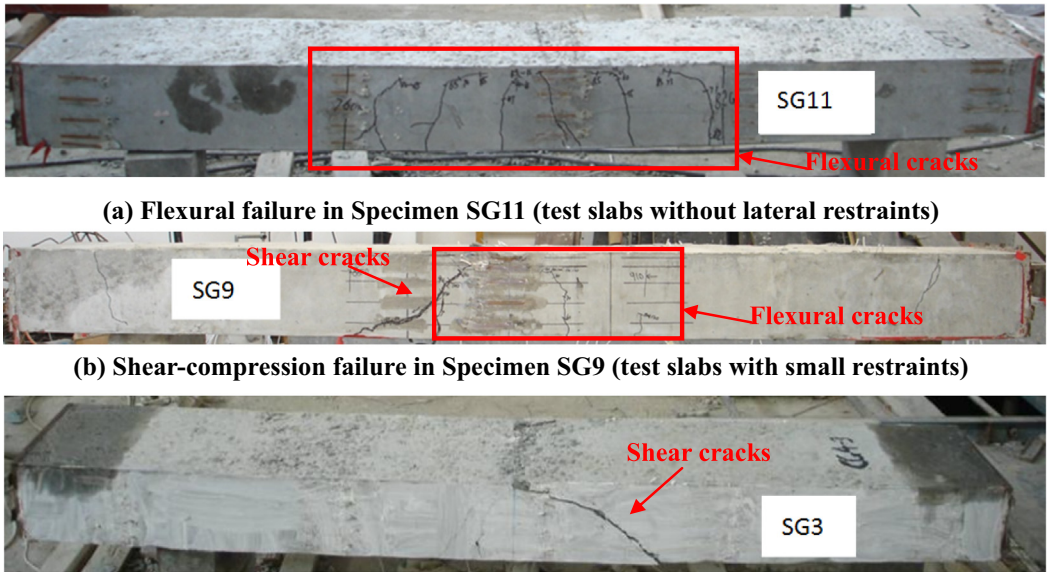

Fig. 7. Failure modes of test slabs with different lateral restraint stiffness at ultimate loads.

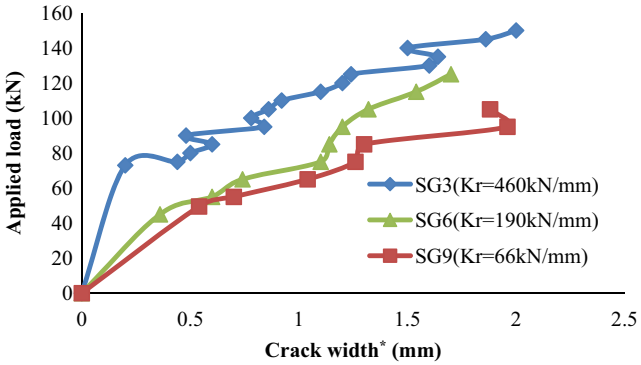

(a) Influence of lateral restraint stiffness

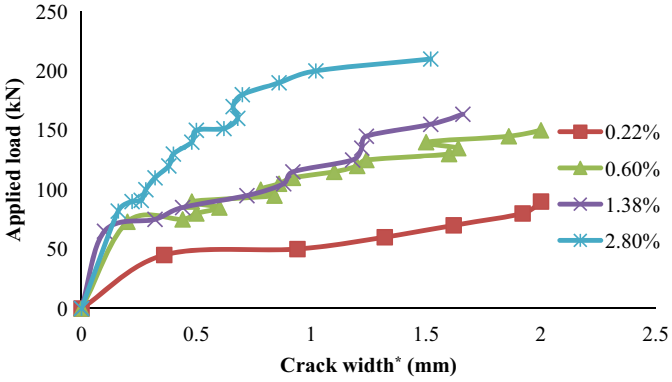

(b) Influence of FRP reinforcement percentage

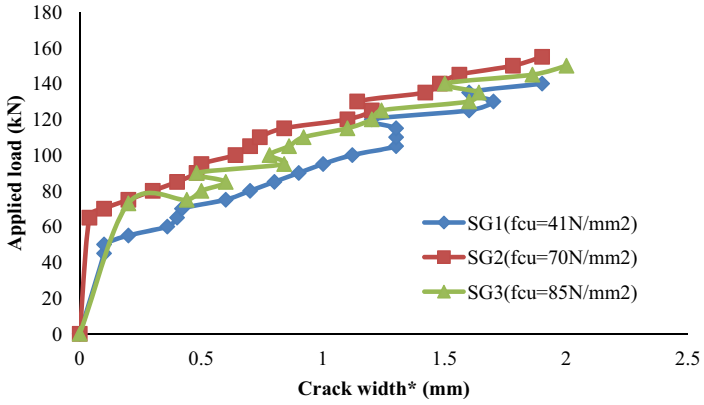

(c) Influence of concrete compressive strength

Fig. 8. Crack width of test slabs vs. applied load crack width* – The measurement of crack width was stopped at the crack width of 2 mm.

second part represents the cracked slab with the reduction stiffness. As shown in Fig. 9a, the specimens had similar stiffness up to the initial flexural crack and followed by a reduction stiffness for all slabs but with different tendencies, which is attributed to the difference in the degree of external restraints. It was shown that the midspan deflections of two slabs, SG10 and SG11, were around five times of those of the restrained slabs at a loading level of 90 kN (see Fig. 9a). On the contrary, Figs. 9b and c illustrate that the reduction of stiffness in load–deflection curves cannot be affected by the variations in other structural variables (concrete strengths, FRP reinforcement ratio and reinforcing material) significantly. This is different from the findings from the test of simply supported FRP reinforced concrete members [8], which could be due to the strong restraint stiffness (460 kN/mm) used in those test slabs.

The horizontal deflections of the steel rigs in the test specimens are shown in Fig. 10. For all the test restrained slabs, it was observed that the horizontal deflections were enhanced significantly as soon as the applied load exceeded the flexural crack loads, which indicated that arching thrust was developed after this loading level. It was expected that the horizontal displacement of the specimen coded as SG3 with large restraint stiffness was smallest among those three slabs (see Fig. 10a). As similar to the load vs. vertical deflection response, this behaviour could not be affected by the variation of concrete strengths (see Fig. 10b). As shown Fig. 10c, increasing the FRP reinforcement percentage resulted in the smaller horizontal deflections in the restrained test slabs with the same restraint stiffness. This could be attributed to the reduced contribution of arching action by increasing the FRP reinforcement percentage [6].

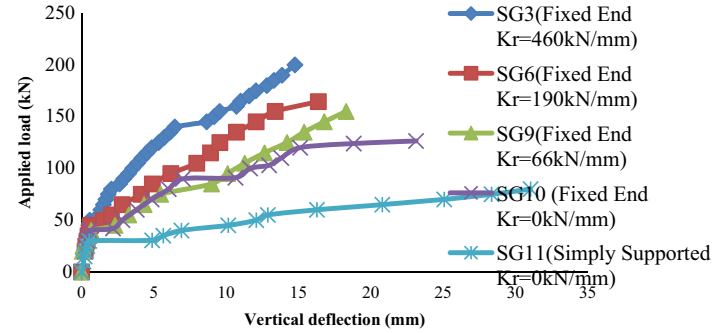

(a) Effect of slab boundary

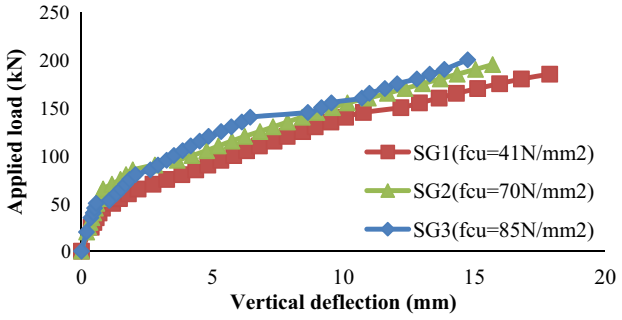

(b) Effect of concrete compressive strength

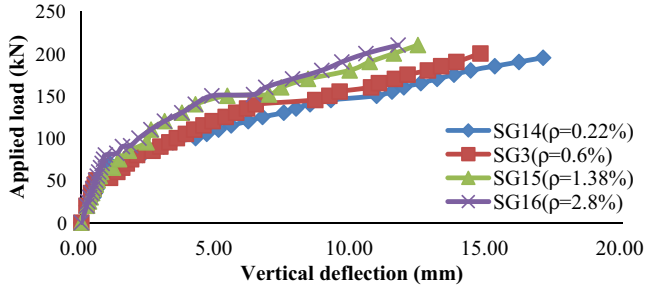

(c) Effect of FRP reinforcement percentage

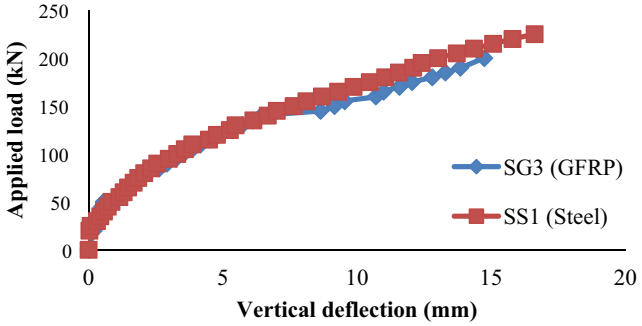

(d) Effect of reinforcing materials

Fig. 9. The response of applied load vs. vertical deflection at the midspan.

4.3. Strain in FRP reinforcement

Fig. 11 shows the applied load versus the FRP reinforcement strain. The strain values are the average measured strain for the longitudinal GFRP bars at the midspan. Initially, the strain values of the GFRP bars in all the test slabs developed in a similar manner before the occurrence of the initial flexural cracks (see Fig. 11). As shown in Fig. 8a, the contribution of FRP reinforcement in the test slabs without restraints was far more significant than that in the restrained test slabs. On the contrary, increasing the concrete strength could not affect the strain of GFRP bars in the restrained slabs significantly as shown in Fig. 11b. Fig. 11c illustrates that the strain measured on the reinforcing GFRP bars is reduced by increasing the reinforcement ratios. In addition, the maximum tensile strain of the GFRP reinforcement in all the restrained test slabs, expect the model coded as SG14 ($\rho = 0.22\%$), was up to 70% of the rupture strain at the ultimate loads.

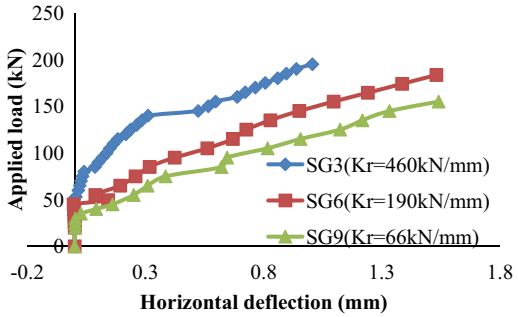

(a) Effect of lateral restraint stiffness

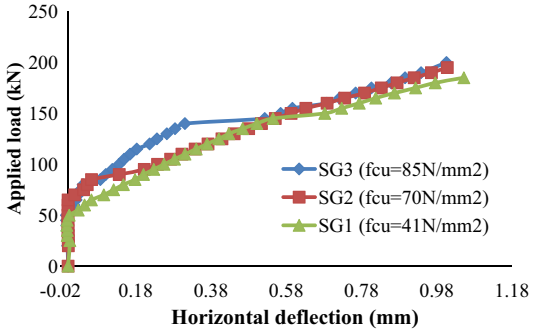

(b) Effect of concrete compressive strength

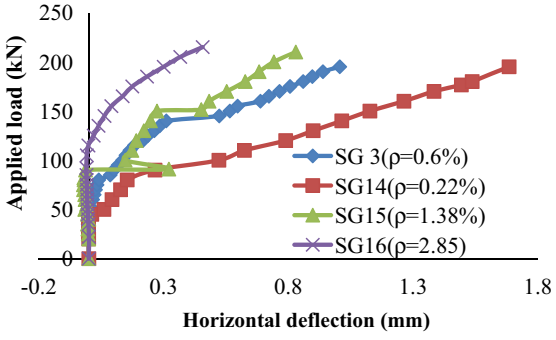

(c) Effect of FRP reinforcement percentage

Fig. 10. The response of the applied load vs. horizontal deflection of steel rig Effect of FRP reinforcement percentage.

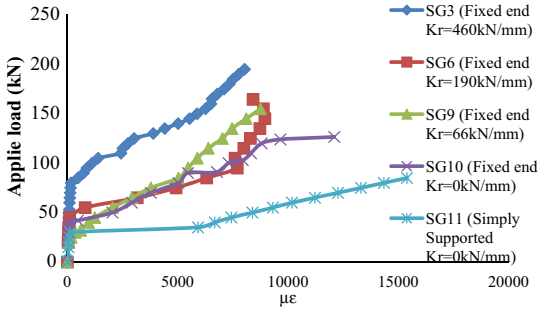

(a) Effect of slab boundary condition

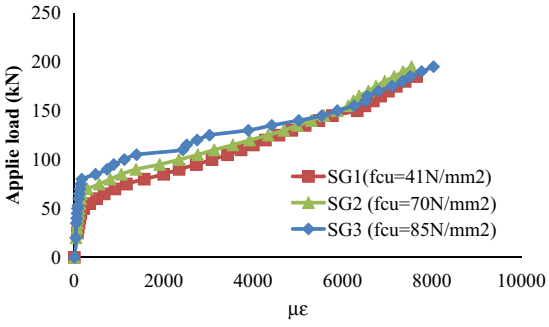

(b) Effect of concrete strength

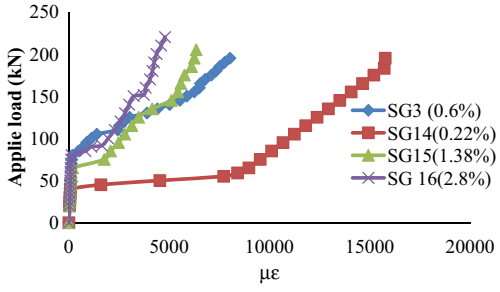

(c) Effect of FRP reinforcement percentage

Fig. 11. The response of applied load vs. strain measured in longitudinal FRP reinforcement.

4.4. Ultimate strength

Table 1 summarises the loading–carrying capacities of the test slabs. As shown in Table 1, all the restrained test slabs failed in shear-compression mode. The effect of several structural parameters on shear failure loads is presented in Fig. 12 graphically. Increasing the degree of external restraint had a strong effect on ultimate shear capacity for the restrained specimens, see Fig. 12a. Comparing the loading–carrying capacities of a restrained slab (SG3) and a simply supported slab (SG11) reveals that the strength is enhanced by more than 50%. This indicates that increasing the restraint stiffness enhances the arching thrust strength and compressive depth [6], which is governing the failure, and in turn increases the transferred shear forces through the arching action. Additionally, the increasing rate of shear strength in each set of the test slabs having similar concrete strength was nearly the same. This is attributed to the similar influence from arching action. Meanwhile, comparing the specimens having the same restraint stiffness reveals the clear effect of concrete compressive strength on the ultimate shear strength as shown in Fig. 12b. Fig. 13c illustrates that increasing the reinforcement ratio from 0.22% to 2.8% has no significant effect on shear strengths for the restrained slabs, which is different from the test results of simply supported FRP reinforced concrete members by other researchers [10,11]. Interestingly, the similar research findings were also presented in the study of restrained slabs reinforced with steel [13] and GFRP reinforced deck slabs [5]. This is attributed to the decreased influence from arching action by increasing the reinforcement percentage [5].

4.5. Parametric study of arching action and FRP reinforcement contribution to shear strength

In this study, the contribution degree of arching action to the shear strengths was investigated by the axial forces in the concrete slabs. The axial forces were calculated from external restraint stiffness (see Table 3 and Eq. (1)) and the horizontal deflections measured in the test (see Fig. 11). Meanwhile, the influence from FRP reinforcement were also represented by the axial forces inside the bars, which were obtained from the measured reinforcement strain (see Fig. 10) and reinforcing material properties (see Table 2). Based on the observation of the test, three critical structural parameters had strong affect on the shear behaviour of test

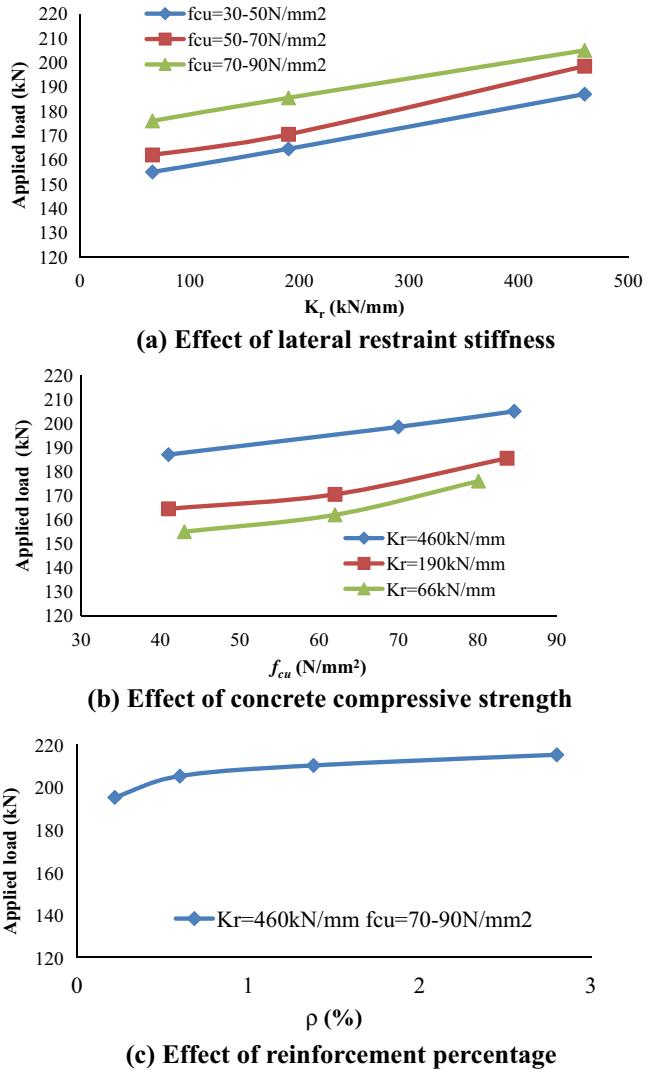

Fig. 12. The effect of structural variables on loading–carrying capacities of the restrained test slabs.

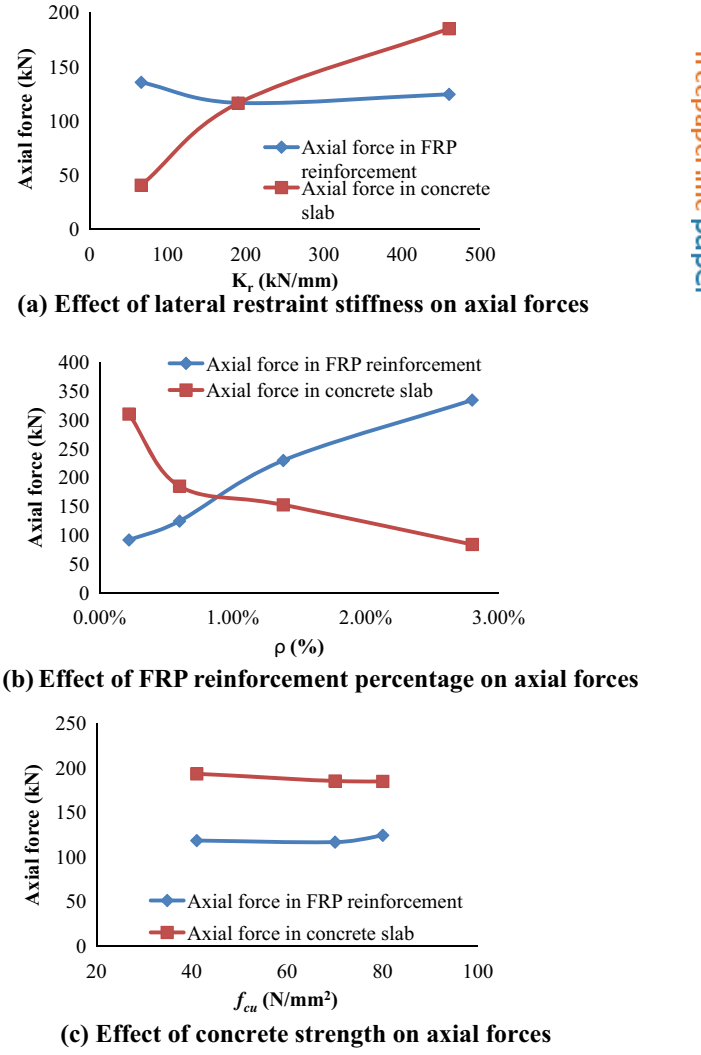

Fig. 13. Comparison of axial forces provided by lateral restraints and in the longitudinal FRP bars with varied structural parameters.

slabs, which included lateral restraint stiffness, concrete strengths and FRP reinforcement ratio. A corresponding parametric study was conducted to investigate the influence of those structural variables on the contribution from arching action and FRP reinforcement as shown in Fig. 13. As shown in Fig. 13a, the axial force in concrete slabs was enhanced as increasing the lateral restraint stiffness. On the other hand, the axial force of FRP reinforcement were reduced slightly by increasing this stiffness values. This indicates that increasing the degree of external restraint resulted in dramatically stronger contribution of arching action and slightly smaller contribution of FRP reinforcement. Hence, the shear strength of restrained FRP reinforced concrete slabs was enhanced by increasing the lateral restraint stiffness significantly (see Fig. 12a). As shown in Fig. 13b, the variation in reinforcement percentage had a strong effect on the influence from arching action and FRP bars simultaneously. It was expected that the contribution of FRP reinforcement was improved as increasing the reinforcement ratio. On the contrary, the effect of arching action on shear capacity was reduced. Interestingly, the increasing rate of axial forces in FRP reinforcement was close to the reducing rate of those at the end of concrete slabs (see Fig. 13b). Under this condition, the ultimate capacity of the restrained slabs could be not be affected by FRP reinforcement percentage significantly (see Fig. 12c). In addition, the contribution of arching action and FRP reinforcement was not affected by increasing the concrete strength as shown in Fig. 13c. This analytical result suggests that any theory for the prediction of the ultimate shear capacity of laterally restrained FRP concrete slabs must take into account the influence of the concrete strength, the FRP reinforcement and the degree of external restraint comprehensively.

5. Comparison of predicted and experimental shear capacities

5.1. Predicted shear capacity by the existing theoretical models

Currently, the shear behaviour of the restrained FRP reinforced concrete members is still less well understood. In the previous study, it was found that some attempts to use the steel reinforced concrete member design provisions unmodified for FRP members produced unconservative prediction results [16]. This implies that a fundamental difference in the shear behaviour between members reinforced with steel and FRP could exist. This structural fact is supported by the findings from the experimental investigations on concrete beams reinforced longitudinal with CFRP and GFRP bars [17]. Those experimental test results also revealed that the axial stiffness of the reinforcing bars was a key parameter in evaluating the concrete shear strength of the flexural member

Table 3
Summary of the existing shear design formulations.

Design procedure	Equation	Variables
ACI 440.1 R-06 [14]	$V_{ACI} = 0.4 \cdot \sqrt{f'_c} \cdot b_w \cdot k \cdot d$ (2)	f'_c – Concrete strength (cylinder test); $k = \sqrt{2 \cdot n_f \cdot \rho_f + (n_f \cdot \rho_f)^2} - n_f \cdot \rho_f$ ρ_f – FRP reinforcement percentage $n_f = E_f / E_c$ E_f – Elastic modulus of FRP reinforcement E_c – Elastic modulus of concrete b_w – Slab web width d – Effective depth of slab
JSCE 1997 [20]	$V_{JSCE} = \beta_d \cdot \beta_p \cdot \beta_n \cdot f_{vud} \cdot b_w \cdot d$ (3)	$\beta_d = (1000/d)^{1/4} \leqslant 1.5$ $\beta_p = (100 \rho_f E_f / E_s)^{1/3} \leqslant 1.5$ $\beta_n = 1$ (No axial forces) $f_{vud} = 0.2 \cdot f_c^{1/3} \leqslant 0.72\ \mathrm{N/mm^2}$
CSA S806-12 [21]	$V_{CSA} = 0.05 \cdot \lambda \cdot \phi_c \cdot k_m \cdot k_r \cdot k_a \cdot k_s \cdot (f'_c)^{1/3} \cdot b_w \cdot d_v$ (4) $0.11 \cdot \phi_c \cdot \sqrt{f'_c} \cdot b_w \cdot d_v \leqslant V_{CSA} \leqslant 0.22 \cdot \phi_c \cdot \sqrt{f'_c} \cdot b_w \cdot d_v$	$k_m = \sqrt{\frac{V_f d}{M_f}} \leqslant 1.0$ $k_r = 1 + (E_f \rho_f)^{1/3}$ $k_a = \frac{2.5}{\frac{M_f}{V_f d}} \geqslant 1.0$ $k_s = \frac{750}{450+d} \leqslant 1.0$ M_f – The factored moment; V_f – The factored shear force $d_v = min(0.9 \cdot d, 0.72 \cdot h)$ λ – Concrete density factor
IStructE 1999 [22]	$V_{IStructE} = 0.79 \cdot \left(\rho_f \cdot \frac{E_f}{E_s}\right)^{1/3} \cdot \left(\frac{400}{d}\right)^{1/4} \cdot \left(\frac{f_{cu}}{25}\right)^{1/3} \cdot b_w \cdot d$ (5)	f_{cu} – concrete strength (cylinder test); E_f – Elastic modulus of FRP reinforcement E_s – Elastic modulus of Steel reinforcement
El-Sayed et al. [23]	$V_{El\text{-}Sayed} = \left(\frac{\rho_f E_f}{90 \beta_1 f'_c}\right)^{1/3} \cdot \left(\frac{\sqrt{f'_c}}{6} b_w d\right)$ (6) $V_{El\text{-}Sayed} \leqslant \frac{\sqrt{f'_c}}{6} \cdot b_w \cdot d$	$0.85 \geqslant \beta_1 = 0.85 - 0.0007 \cdot (f'_c - 28) \geqslant 0.65$
Kara [24]	$V_{Kara} = \left(\sqrt[3]{\frac{d}{a}} \cdot f_c \cdot \frac{\rho_f \cdot E_f}{E_s} \cdot \left(\frac{c_1^2}{c_0}\right)\right)^{1/3} \cdot \frac{c_0}{c_2} \cdot b_w \cdot d$ (7)	a – Shear span c_0 – Constant equal to 7.696 c_1 – Constant equal to 7.254 c_2 – Constant equal to 7.718
Alam and Hussein [25]	$V_{Alam} = \frac{0.2\lambda}{a/d} \cdot \left(\frac{\rho_f E_f}{d}\right)^{1/3} \cdot \sqrt{f_c} \cdot b_w \cdot d$ (8) $\frac{0.1\lambda}{a/d} \cdot \sqrt{f'_c} \cdot b_w \cdot d \leqslant V_{Alam} \leqslant \frac{0.2\lambda}{a/d} \cdot \sqrt{f'_c} \cdot b_w \cdot d$	λ – Concrete density factor
Hoult et al. [26]	$V_{Hoult} = \frac{0.3}{0.5+(0.15+1000\epsilon_x)^{0.7}} \cdot \frac{1300}{(1000+s_{xe})} \cdot \sqrt{f'_c} \cdot b_w \cdot d_v$ (9)	$\epsilon_x = \frac{M_f/d_v + V_f}{2 \cdot E_f \cdot A_f}$ $s_{xe} = \frac{31.5d}{16+a_g} \geqslant 0.77d$ M_f – Bending moment at the critical section for shear; V_f – Shear force at the critical section for shear a_g – Maximum aggregate size in mm
Abdul-Salam [27]	$V_{Abdul\text{-}Salam} = 0.018 \cdot \left(\frac{a}{d}\right)^{1/4} \cdot \left(1 + \sqrt[3]{E_f \rho_f}\right) \cdot d \cdot b_w \cdot \sqrt[3]{f'_c}$ (10)	
Antonio et al. [28]	$V_{Antonio} = v_{u,t} \cdot f_{ct} \cdot b_w \cdot d$ (11) $v_{u,t} = \xi \cdot (1.072 - 0.01 \cdot \alpha) \cdot \frac{c_1}{d} + 0.036$	$\alpha = \frac{E_f}{E_c}$ $\frac{c_1}{d} = \alpha \cdot \rho_f \cdot \left(1 + \sqrt{1 + \frac{2}{\alpha \cdot \rho_f}}\right)$ $\xi = 1.2 - 0.2 \cdot a,\ a\ in\ m$

reinforced by FRP bars. Therefore, some researchers developed new shear-strength prediction models taking into account the difference in modulus of elasticity of FRP reinforcement [11,18]. In this paper, the shear capacity of the restrained concrete slabs reinforced with GFRP bars were predicted by using shear equations of design codes [14,19–21] and theoretical models from literatures [22–27] to study the accuracy of those existing shear design methods. Table 3 summarises the shear-strength prediction equations from those literatures [14,19–27]. It can be found that most of those formulations were developed by modifying the existing shear design equations for steel reinforced concrete structures.

The predicted shear capacities of the restrained test slabs by the design equations from the current FRP reinforced concrete design codes [14,19–21] and literatures [22–27] were shown in Tables 4 and 5 respectively. It was evident that those existing theoretical models yielded high conservative predicted shear strengths and the reliability of those predictions was not good. As shown in Tables 4 and 5, the average ratios of the predicted capacity (V_p) to the test capacity (V_{test}) are from 0.34 to 0.71. In addition, the COV values of all the ratios of V_p/V_{test} are around 20% for those prediction methods. In the analytical study of those theoretical models, it was found that the effect of arching action was not incorporated into the design equations due to the large shear span-to-depth ratio ($\geqslant 2.5$). In addition, despite the 60 N/mm^2 concrete strength limit in the CSA-S806-12 shear-strength provision [20], this method yielded better predictions for those test slabs compared to the results from other equations (see Tables 4 and 5).

In the study of FRP reinforced concrete bridge decks [5], it was shown that the arching effect was improved by increasing the

Table 4
Comparison of the predicted shear capacity by current design codes [14,20–22] with the test results.

Model	V_{test} (kN)	V_{ACI} (kN)	V_{JSCE} (kN)	V_{CSA} (kN)	$V_{IStructE}$ (kN)	V_{ACI}/V_{test}	V_{JSCE}/V_{test}	V_{CSA}/V_{test}	$V_{IStructE}/V_{test}$
SG1	176	37	61	109	74	0.21	0.35	0.62	0.42
SG2	199	42	68	142	89	0.21	0.34	0.72	0.45
SG3	205	44	68	156	94	0.22	0.33	0.76	0.46
SG4	165	37	61	109	74	0.22	0.37	0.66	0.45
SG5	171	41	68	134	85	0.24	0.40	0.79	0.50
SG6	186	44	68	156	94	0.24	0.37	0.84	0.51
SG7	143	37	62	111	75	0.26	0.43	0.78	0.53
SG8	156	41	68	134	85	0.26	0.44	0.86	0.55
SG9	176	44	68	152	93	0.25	0.39	0.86	0.53
SG12	199	44	68	156	94	0.22	0.34	0.79	0.48
SG13	195	35	50	58	79	0.18	0.26	0.30	0.40
SG14	195	28	49	124	68	0.14	0.25	0.64	0.35
SG15	210	65	91	151	123	0.31	0.43	0.72	0.58
SG16	215	85	113	144	148	0.39	0.53	0.67	0.69
Average =						0.24	0.37	0.71	0.49
Standard deviation =						0.06	0.07	0.14	0.08
Coefficient variation =						0.25	0.19	0.20	0.17

Table 5
Comparisons of the predicted shear capacity from literatures [23–28] with the test results.

Model	V_{test} (kN)	$V_{El\text{-}Sayed}$ (kN)	V_{Kara} (kN)	V_{Alam} (kN)	V_{Hoult} (kN)	$V_{Abdul\text{-}Salam}$ (kN)	$V_{Antonio}$ (kN)	$V_{El\text{-}Sayed}/V_{test}$	V_{Kara}/V_{test}	V_{Alam}/V_{test}	V_{Hoult}/V_{test}	$V_{Abdul\text{-}Salam}/V_{test}$	$V_{Antonio}/V_{test}$
SG1	176	56	67	50	56	84	73	0.32	0.38	0.28	0.32	0.48	0.42
SG2	199	62	81	65	66	101	94	0.31	0.41	0.33	0.33	0.51	0.47
SG3	205	64	86	71	70	111	103	0.31	0.42	0.35	0.34	0.54	0.50
SG4	165	56	67	50	56	84	73	0.34	0.41	0.30	0.34	0.51	0.45
SG5	171	60	77	61	63	97	89	0.35	0.45	0.36	0.37	0.57	0.52
SG6	186	64	86	71	69	111	102	0.34	0.46	0.38	0.37	0.60	0.55
SG7	143	57	69	51	56	86	75	0.40	0.48	0.36	0.39	0.60	0.53
SG8	156	60	77	61	63	97	89	0.39	0.50	0.39	0.41	0.62	0.57
SG9	176	63	84	69	69	109	100	0.36	0.48	0.39	0.39	0.62	0.57
SG12	199	64	86	71	70	111	103	0.32	0.43	0.36	0.35	0.56	0.52
SG13	195	47	60	45	45	91	80	0.24	0.31	0.23	0.23	0.47	0.41
SG14	195	46	62	52	48	85	71	0.24	0.32	0.27	0.25	0.43	0.37
SG15	210	84	111	91	94	139	144	0.40	0.53	0.44	0.45	0.66	0.69
SG16	215	102	134	109	115	171	189	0.48	0.62	0.50	0.53	0.80	0.88
Average =								0.34	0.44	0.35	0.36	0.57	0.53
Standard deviation =								0.06	0.08	0.07	0.08	0.09	0.13
Coefficient variation =								0.18	0.18	0.20	0.21	0.16	0.24

lateral restraint stiffness and decreased by the enhancement of reinforcement percentage. The similar structural behaviour was also obtained in this test study as illustrated in Figs. 13a and b. Therefore, the ratios of the predicted shear capacity (V_p) to the test capacity (V_{test}) are plotted against FRP reinforcement percentage and lateral restraint stiffness respectively, see Figs. 14 and 15. As illustrated in Fig. 14, increasing the reinforcement percentage could improve the accuracy of the prediction method. On the other hand, increasing the lateral restraint stiffness resulted in smaller ratios of V_p to V_{test} see Fig. 15. Based on this analytical result, it can be summarised that the contribution of arching action should be incorporated into the shear-strength prediction methods for the laterally restrained GFRP reinforced concrete members.

5.2. Predicted shear capacity with introduction of arching action

In the experimental study, it was shown that the influence of arching action on the shear behaviour of restrained test slabs were similar to the over-reinforcing effect in concrete members (see Fig. 7). Therefore, the effect of arching action on shear capacity could be assumed to be equivalent to increasing the reinforcement percentage. This theoretical assumption was also used by Kirkpatrick et al. [28] and BD 81/02 [29] in the study of shear punching capacity of concrete bridge deck slabs. Because this equivalent arching reinforcement percentage [28,29] was developed empirically based on the test results of steel reinforced concrete structures, a stiffness coefficient of $\frac{E_f}{E_s}$ should be introduced. Using this stiffness coefficient, the "equivalent" FRP reinforcement percentage [29] can be obtained as below:

$$\rho'_a = \frac{E_f}{E_s} \cdot \frac{k_a \cdot f_c \cdot h^2}{320 \cdot d^2} \tag{12}$$

where k_a is the maximum arching moment coefficient as follow:

$$k_a = 0.0525 \cdot (4.3 - 16.1\sqrt{3.3 \cdot 10^{-4} + 0.1234 \cdot R}) \tag{13}$$

In Eq. (13), R is a measure of the elastic deformation that is as defined in Eq. (14).

$$R = \frac{\varepsilon'_c \cdot L_r}{h^2} \tag{14}$$

In Eq. (14), ε'_c is the plastic strain of an idealised elastic–plastic concrete, which is given by

$$\varepsilon'_c = (-400 + 60 \cdot f_c - 0.33 \cdot f_c) \times 10^{-6} \tag{15}$$

Furthermore, L_r is the half span of the equivalent rigidly restrained arch (see Eq. (16)), which was provided by Rankin [30] with idealisation of the slab as a three-hinged arch [31].

$$L_r = a \cdot \sqrt[3]{\frac{E_c \cdot b_w \cdot d}{K_r \cdot a} + 1} \tag{16}$$

where a is the shear span, K_r is the lateral restraint stiffness.

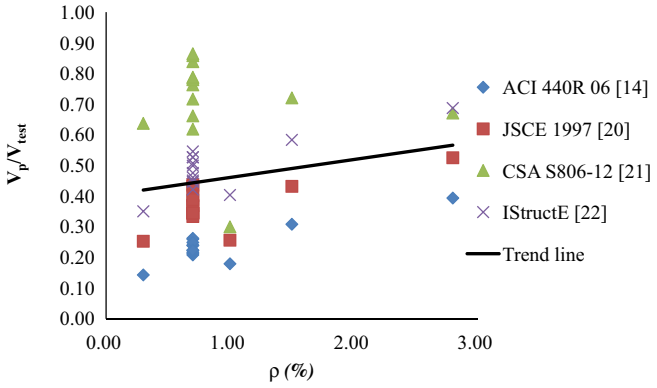

(a) The shear capacity predicted by current design codes

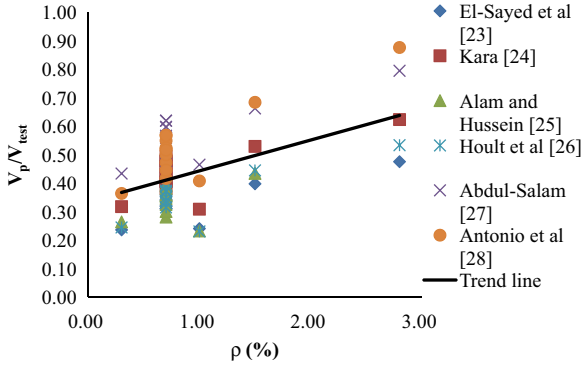

(b) The shear capacity predicted by design equations in literatures

Fig. 14. The ratios of the predicted shear capacity to the test capacity vs. FRP reinforcement percentage.

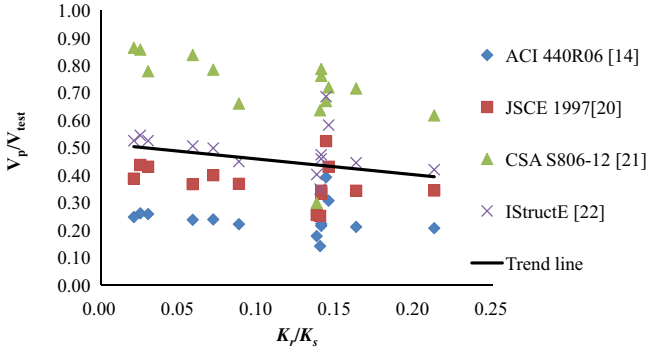

(a) The shear capacity predicted by current design codes

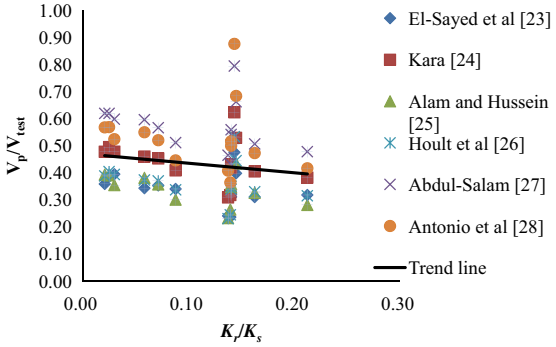

(b) The shear capacity predicted by design equations in literatures

Fig. 15. The ratios of the predicted shear capacity to the test capacity vs. lateral restraint stiffness (Ks – The axial stiffness of concrete slabs strip).

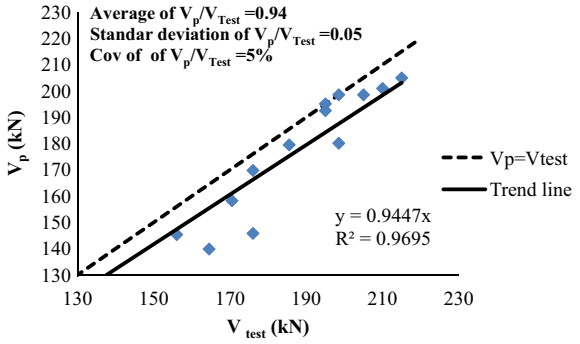

Fig. 16. The predicted shear capacity by the modified method vs. the test results.

Thus, the proposed equation herein takes into account this arching reinforcement to predict the shear capacity of the restrained FRP reinforced concrete slabs. The "equivalent" reinforcement percentage was proposed by Kirkpatrick et al. [28] for the prediction method in British Standard 5400 [32], which is similar to the shear-strength equation of IStructE 1999 [21]. Therefore, the proposed equation in this paper is a modification of the IStructE 1999 [21] method by adding this "equivalent" reinforcement percentage as shown as Eq. (17).

$$V_{IStructE} = 0.79 \cdot \left(\rho_f \cdot \frac{E_f}{E_s} + \rho'_a\right)^{1/3} \cdot \left(\frac{400}{d}\right)^{1/4} \cdot \left(\frac{f_{cu}}{25}\right)^{1/3} \cdot b_w \cdot d \quad (17)$$

The shear capacities of the restrained GFRP reinforced concrete slabs in this experimental study are plotted against the predicted values by Eq. (17) in Fig. 16. The trend line is fitted to the data using regression analysis. It can be seen that the slope of the trend line is equal to 0.94 and the R^2 value of the regression line is 0.97. In the comparison with the test results, the proposed method yielded accurate and slightly conservative predictions with an average V_p/V_{test} of 0.94 and a corresponding COV of 5%.

6. Conclusions

The shear behaviour of one-way laterally restrained concrete slabs reinforced with GFRP bars was investigated in this paper. The influence from arching action on the shear behaviour was presented and discussed. The variables considered in the test were lateral restraint stiffness, concrete strength and reinforcement configurations. The experimental shear-strength results were compared to the available shear design equations and the proposed shear-strength prediction method. Based on the results obtained in this study, the following conclusions can be drawn:

(1) Due to the existence of lateral restraints, all the restrained GFRP reinforced concrete slabs failed in shear. The observed failure mode was shear-compression. However, flexural failure was observed in the test slabs without lateral restraints due to the low reinforcement percentage (0.6%) and large span-to-depth ratio ($\geqslant 6$).

(2) The experimental evidence indicated that the contribution of arching action to shear behaviour was similar to increasing the reinforcement percentage. Increasing the arching effect trended to increase the shear strength by delaying cracking and limiting the penetrated depth of the crack into the slabs. The enhancement in the shear capacity was due to the improvement of the shear transfer and the increased area of compression concrete.

(3) In the study of axial forces in concrete slabs and those occurring in the longitudinal GFRP bars, it was found that the contribution of arching action to shear strengths was enhanced by increasing the lateral restraint stiffness and reducing the FRP reinforcement percentage. However, the variation of concrete strength could not affect the arching effect significantly.

(4) This paper evaluated the performance of several design codes and design equations of literatures in the shear-strength prediction of the restrained GFRP reinforced concrete slabs. The effect of arching action on the shear capacity was not considered by those theoretical methods due to the large span-to-depth ratio. Therefore, the analytical results showed that all the existing shear-strength prediction methods yielded high conservative prediction results.

(5) Based on the study of arching action in the laterally restrained deck slabs [5,28], an "equivalent" arching reinforcement percentage was adopted to take into account the arching action contribution to the shear strength. A modification of the shear-strength prediction method of IStructE 1999 [21] was proposed by adding this arching reinforcement percentage. The proposed equation was applied to calculate the shear capacities of the restrained test slabs and yielded accurate and slightly conservative prediction results.

Acknowledgements

The authors wish to express their sincere appreciation of the Foundation of Guangdong Distinguished Young Scholar Planning (Yq2013155), the National Natural Science Foundation of China (50908055) and Division of Transportation Guangdong Province (2013-02-029) in supporting this research.

References

[1] Domenico DD, Pisano AA, Fuschi P. A FE-based limit analysis approach for concrete elements reinforced with FRP bars. Compos Struct 2014;107:594–603.
[2] Anoop MB, Rao KB, Rao TVSRA. Application of fuzzy sets for estimating service life of reinforced concrete structural members in corrosive environments. Eng Struct 2002;24(9):1229–42.
[3] Benmokrane B, El-Salakawy E, El-Ragaby A, Lackey T. Designing and testing of concrete bridge decks reinforced with glass FRP bars. J Bridge Eng 2006;11(2):217–29.
[4] Vaz Rodrigues R. Shear strength of reinforced concrete bridge deck slabs [Ph.D. thesis]. Lausanne, Switzerland: École Polytechnique Fédérale de Lausanne; 2007.
[5] Zheng Y, Yu GY, Pan YF. Investigation of ultimate strengths of concrete bridge deck slabs reinforced with GFRP bars. Constr Build Mater 2012;28:482–92.
[6] Zheng Y, Li CH, Yu GY. Investigation of structural behaviours of laterally restrained GFRP reinforced concrete slabs. Compos: Part B-Eng 2012;438(2):1586–97.
[7] Taylor SE, Mullin B. Arching action in FRP reinforced concrete slabs. Constr Build Mater 2006;20:71–80.
[8] El-Sayed AK. Concrete contribution to the shear resistance of FRP reinforced concrete beams [Ph.D. thesis]. Canada: Sherbrooke University; 2006.
[9] Zheng Y, Sun C, Yang JB, Deng T, Lu ZY. Arching action contribution to punching failure of GFRP reinforced concrete bridge deck slabs. Arab J Sci Eng 2014;39(12):8609–25.
[10] El-Sayed A.K. Concrete contribution to the shear resistance of FRP reinforced concrete beams [Ph.D. thesis]. Canada: Sherbrooke University; 2006.
[11] El-Sayed AK, El-Salakawy E, Benmokrane B. Shear strength of one-way concrete slabs reinforced with fiber-reinforced polymer composite bars. J Compos Constr 2005;9(2):147–57.
[12] Zheng Y. Modelling of compressive membrane action in bridge decks [Ph.D. thesis]. United Kingdom: Queen's University Belfast; 2008.
[13] Taylor SE, Rankin GIB, Cleland DJ. Arching action in high strength concrete slabs. ICE Proc—Struct Build 2001;146(4). 353-262.
[14] American Concrete Institute (ACI). Guide for the design and construction of concrete reinforced with FRP bars. ACI 440.1R-06, Farmington Hills, Mich; 2006.

[15] Tharmarajah G, Taylor SE, Robinson D, Cleland D. Corrosion resistant fibre reinforced polymer (FRP) reinforcement for bridge deck slabs. In: Proceedings of the ICE – Bridge Eng; 2014. Available online.
[16] Yost JR, Gross SP, Dinehart DW. Shear strength of normal strength concrete beams reinforced with deformed GFRP bars. J Compos Constr 2001;5(4):268–75.
[17] El-Sayed, AK, El-Salakawy EF, Benmokrane B. Evaluation of concrete shear strength for beams reinforced with FRP bars. In: 5th structural specialty conference of the Canadian society for civil engineering, CSCE. Canada: Saskatoon, Saskatchewan; June 2–5 2004 (on CD-Rom), 10 p.
[18] Tureyen A, Frosch RJ. Shear tests of FRP-reinforced beams without stirrups. ACI Struct J 2002;99(4):427–34.
[19] Japan Society of Civil Engineers (JSCE). Recommendation for design and construction of concrete structures using continuous fiber reinforcing materials concrete engineering series no. 23; 1997: p. 325.
[20] Canadian Standards Association, Design and construction of building components with fibre reinforced polymers, CSA-S806-02, Rexdale, Ontario, Canada, 202 p. Canadian Standards Association, 2012. Design and Construction of Building Components with Fibre Reinforced Polymers, (CSA-S806-12), Rexdale, ON, Canada.
[21] Institute of Structural Engineers (IStructE). Interim guidance of the design of reinforced concrete structures using fibre composite reinforcement, Published by SETO Ltd, London, United Kingdom; 1999.
[22] El-Sayed AK, El-Salakawy EF, Benmokrane B. Shear strength of concrete beams reinforced with FRP bars: design method. ACI Struct J Spec Publ 2005;230:955–74.
[23] Kara IF. Prediction of shear strength of FRP-reinforced concrete beams without stirrups based on genetic programming. Adv Eng Softw 2011;42:295–304.
[24] Alam MS, Hussein A. Unified shear design equation for FRP reinforced concrete members without stirrups. J Compos Constr 2013;17(5):575–83.
[25] Hoult NA, Sherwood EG, Bentz EC, Collins MP. Does the use of FRP reinforcement change the one-way shear behavior of reinforced concrete slabs? J. Compos. Constr. 2008;12(2):125–33.
[26] Abdul-Salam B. Behaviour of shear critical FRP reinforced concrete one-way slabs [Ph.D. thesis]. Canada: Sherbrooke University; 2014.
[27] Antonio M, Antoni C, Eva O, Jesús B. Shear design of FRP reinforced concrete beams without transverse reinforcement. Compos: Part B 2014;57:228–41.
[28] Kirkpatrick J, Rankin GIB, Long AE. Strength evaluation of M-beam bridge deck slabs. The Struct Engr 1984;62(3):60–8.
[29] UK Highways Agency, BD 81/02: Use of compressive membrane action in bridge decks, Design Manual for Roads and Bridges, V. 3, Section 4, Part 20; Aug. 2002, p. 20.
[30] Rankin GIB. Punching failure and compressive membrane action in reinforced concrete slabs [Ph.D. thesis]. Northern Ireland, United Kingdom: Queen's University Belfast; 1982: p. 56–106.
[31] Lind NC, Puranik B. The stability analysis of reticulated domes with grid discontinuities. In: Davies RM, editor. Space structures. Blackwell Scientific Publications; 1966. p. 439–43 [chapter 39].
[32] British Standards Institute, BS 5400: Parts 2 & 4, British Standard for the design of steel, concrete and composite bridges, London; 1978 and 1990.